Journal of
Scientific
Exploration
Anomalistics
and
Frontier
Science

RESEARCH ARTICLE

Citizen Orb Photometry Pipeline (COPP): A Standardized Method for Computational Analysis of Anomalous Luminous Phenomena from Consumer Video Captures

Paola Di Maio
Epistemic Systems Lab, Ronin Institute for Independent Scholarship, Edinburgh, United Kingdom
paola.dimaio@ronin-institute.org
orcid.org/0000-0003-0770-3713

SUBMITTED February 10, 2026
ACCEPTED May 26, 2026
PUBLISHED September 29, 2026

https://doi.org/10.31275/20263985

GOLD OPEN ACCESS

ABSTRACT

We present the Citizen Orb Photometry Pipeline (COPP), a standardized ten-step computational method for quantitative analysis of anomalous luminous phenomena (ALP) captured in consumer video recordings. The pipeline extracts frame-by-frame photometric measurements including centroid position, apparent size, peak and integrated intensity, RGB spectral channel decomposition, and derived metrics including blue excess, pulsation periodicity, and position discontinuities. A key methodological innovation is adaptive spectral measurement: when sensor saturation renders core color data unreliable, the pipeline automatically shifts spectral analysis to the unsaturated halo region, enabling consistent cross-case comparison regardless of source brightness or observer distance. We demonstrate COPP through comparative analysis of three ALP captures spanning fourteen years, three countries, and distinct observational conditions: a distant, mobile, spectrally cool orb over the Taiwan coast (2021); a close-range, stationary, spectrally warm orb in the United Kingdom (2011); and a close-range, stationary orb with correlated size-color pulsation in Poland (2025). Despite differences in apparent brightness, angular size, and sensor saturation state, all three cases exhibit spectral overlap consistent with a common emission mechanism. Signal structure analysis of the Taiwan case reveals strong size-intensity correlation ($r = 0.808$) and quasi-periodic pulsation, indicating non-random temporal structure. COPP addresses a documented gap between professionally calibrated instruments and citizen capture platforms by providing a standardized computational bridge that runs in standard Python environments and processes any consumer video format. The COPP v1.0 pipeline demo is available as a working prototype at https://copp-w.vercel.app/. The purpose of this paper is to place the method and its outputs in the public domain in a form others can inspect, critique and extend, and we invite the community to test the pipeline against their own captures and to help make it more reliable and more consistent.

KEYWORDS

Anomalous luminous phenomena, citizen science, photometry, computational analysis, orb, Hessdalen, plasma, spectral analysis, signal processing, UAP.

Anomalous luminous phenomena (ALP) have been documented across diverse geographic and cultural contexts for centuries, yet remain poorly characterized by mainstream science. Among the most systematically studied instances are the Hessdalen lights of central Norway, where persistent luminous phenomena have been observed since the 1980s and subjected to rigorous instrumental investigation (Strand, 1984; Teodorani, 2004; Hauge, 2010). These investigations have established key physical parameters: radiant powers reaching 19 kW, thermal spectra in the visible range, quasi-periodic intensity modulation, and anomalous kinematic behavior including sudden acceleration and position discontinuities (Teodorani, 2004).

Despite this professional work, a fundamental asymmetry persists in the field. Instrumental monitoring stations such as the Hessdalen Automatic Measurement Station (AMS) and calibrated spectrographic equipment are restricted to fixed locations and require significant technical expertise and financial investment. Meanwhile, the vast majority of ALP observations worldwide are captured on consumer devices (smartphones, dashcams, security cameras) by untrained observers who lack tools to extract quantitative information from their recordings. As Morgan and Tyson (2024) note in their analysis of Australian orb phenomena, photometric equipment remains a critical missing component in field investigation protocols.

Several citizen science platforms address portions of this gap. Project Hessdalen maintains a public archive of automated station captures dating to 1998. Sky360 operates an open-source detection network for automated sky monitoring. NASA's Spritacular project crowdsources observations of transient luminous events. However, none of these platforms provide an automated, standardized tool for citizens to perform quantitative photometric analysis of their own video recordings after capture.

This paper presents the Citizen Orb Photometry Pipeline (COPP), a ten-step computational method designed to fill this gap. COPP processes any consumer video recording containing a luminous anomaly and produces standardized photometric measurements suitable for scientific comparison. We illustrate the pipeline through comparative analysis of three independent ALP captures, demonstrating both the method's behavior across diverse observational conditions and the scientific value of the data it extracts.

RELATED WORK

Professional ALP Investigation

The Hessdalen phenomenon represents the gold standard for systematic ALP investigation. Teodorani (2004) conducted calibrated spectroscopic and photometric measurements over multiple field campaigns, establishing that the Hessdalen lights exhibit thermal spectra with temperatures in the range of 6000–9000 K, radiant powers of 19 kW or more, and spectral characteristics consistent with high-temperature plasma. Hauge (2010) described the design and operation of the Hessdalen AMS, an automated monitoring station employing calibrated cameras, magnetometers, and radar, operational since 1998 and archiving observations on a continuous basis. Knuth et al. (2025) extended this work in a multi-author analysis of UAP propulsion characteristics, with Teodorani as co-author, integrating kinematic analysis with spectral data.

In Australia, Morgan and Tyson (2024) documented orb phenomena using multi-instrument field recordings, finding correlations between orb orientation and electromagnetic field buildup, and explicitly calling for standardized photometric measurement protocols. Paiva (2021) proposed an electrically active inversion layer model for Hessdalen-type phenomena, suggesting atmospheric electrical processes as a generation mechanism.

Barbi (2025) demonstrated the application of classical mechanics analysis to video recordings of a luminous object interacting with a missile over Yemen, showing that frame-by-frame analysis of consumer-grade footage can yield physically meaningful kinematic parameters.

Citizen Science Platforms

Existing citizen science platforms for ALP observation fall into three categories: automated detection (Sky360, NASA Spritacular), archival and cataloging (Project Hessdalen, NUFORC, MUFON, GEIPAN), and manual forensic analysis (individual investigators and media analysts). An emerging fourth category involves systematic high-volume capture with consumer-grade enhanced sensors such as night-vision cameras. None of these provide automated post-capture photometric analysis tools for citizen use.

The Gap

The gap COPP addresses is specific and well-defined: it lies between professional calibrated instruments (which produce high-quality data but are geographically and financially restricted) and citizen capture platforms (which collect vast quantities of recordings but lack quantitative analysis capabilities). COPP provides a standardized computational bridge, enabling any citizen with a video recording and a Python environment to extract photometric measurements in the same format used by professional researchers.

METHOD: THE CITIZEN ORB PHOTOMETRY PIPELINE

The Citizen Orb Photometry Pipeline COPP is implemented as a Python module using standard scientific computing libraries (NumPy, SciPy, Matplotlib, Pillow). The pipeline processes consumer video recordings through ten sequential steps, producing per-frame photometric measurements and derived temporal metrics. The method is designed to handle the two principal challenges of citizen ALP video analysis: variable video formats and quality, and the wide range of source brightness from sub-threshold faint to sensor-saturating bright. In the pre-loop phase, which executes once per video, the pipeline extracts all frames and detects the active content region. A per-frame loop then applies adaptive brightness thresholding calibrated to each frame's scene darkness, groups threshold-exceeding pixels into connected clusters, identifies the primary luminous source, and—when a source is detected—computes morphometric, intensity, and adaptive spectral measurements, appending results to a running data structure before advancing to the next frame. Frames in which no source meets the detection criteria are recorded as non-detections and bypass Steps 6 through 8. Once all frames have been processed, the post-loop phase computes derived temporal metrics—including FFT power spectrum estimation, autocorrelation, Runs test non-randomness testing, size-intensity cross-correlations, and burst episode detection—operating on the full assembled time series rather than individual frames. The pipeline concludes by aggregating all measurements into three standardized outputs: a per-frame CSV data table, a photometric dashboard, and a signal structure analysis dashboard. The complete pipeline workflow is presented in Figure 1 using ISO 5807 flowchart notation.

The steps in the pipeline are described in detail in Steps 1 through 10 below.

Step 1: Frame Extraction

Video files are decoded to individual PNG frames using FFmpeg at a configurable target frame rate (default: variable frame rate preservation). This step normalizes across container formats (MP4, WebM, AVI, MOV) and codecs (H.264, VP8, VP9), accepting any consumer video source.

Step 2: Content Region Detection

Many citizen video sources are screen recordings of original captures, or include video player UI overlays, borders, or other non-content elements. COPP automatically detects the content region by analyzing row and column mean brightness profiles. Bright UI elements (toolbars, player controls, window borders) produce characteristic high-brightness bands at frame edges, while the actual video content (typically a dark sky scene) occupies the interior. The content region is defined as the largest contiguous rectangle with mean brightness below an adaptive threshold. A sanity check ensures the detected region comprises at least 30% of the total frame area; if not, the full frame is used.

Step 3: Adaptive Brightness Thresholding

A critical innovation in COPP is the three-tier adaptive threshold for source detection, calibrated to the background brightness of each frame. For ultra-dark scenes [median brightness < 5 digital number (DN), the raw 8-bit pixel value in each channel], such as nighttime ocean or sky observations, the threshold is set at median + 15 DN (minimum 15 DN), providing sensitivity to faint sources. For dark scenes (median 5–30 DN), the threshold is median + 25 DN (minimum 30 DN). For normal scenes (median > 30 DN), the threshold is median + 40 DN (minimum 50 DN). This tiered approach ensures that the same pipeline code detects both faint distant sources (such as the Taiwan case, where peaked at 255 DN in a single channel against a background of 1 DN) and bright nearby sources (such as the UK and Poland cases, where sources saturated the sensor at 255 DN per channel).

Step 4: Connected-Component Labeling

Pixels exceeding the adaptive threshold are grouped into spatially connected clusters using SciPy's ndimage label function with default 4-connectivity. This identifies discrete luminous sources within the frame, distinguishing the primary ALP source from background stars, reflections, or noise clusters.

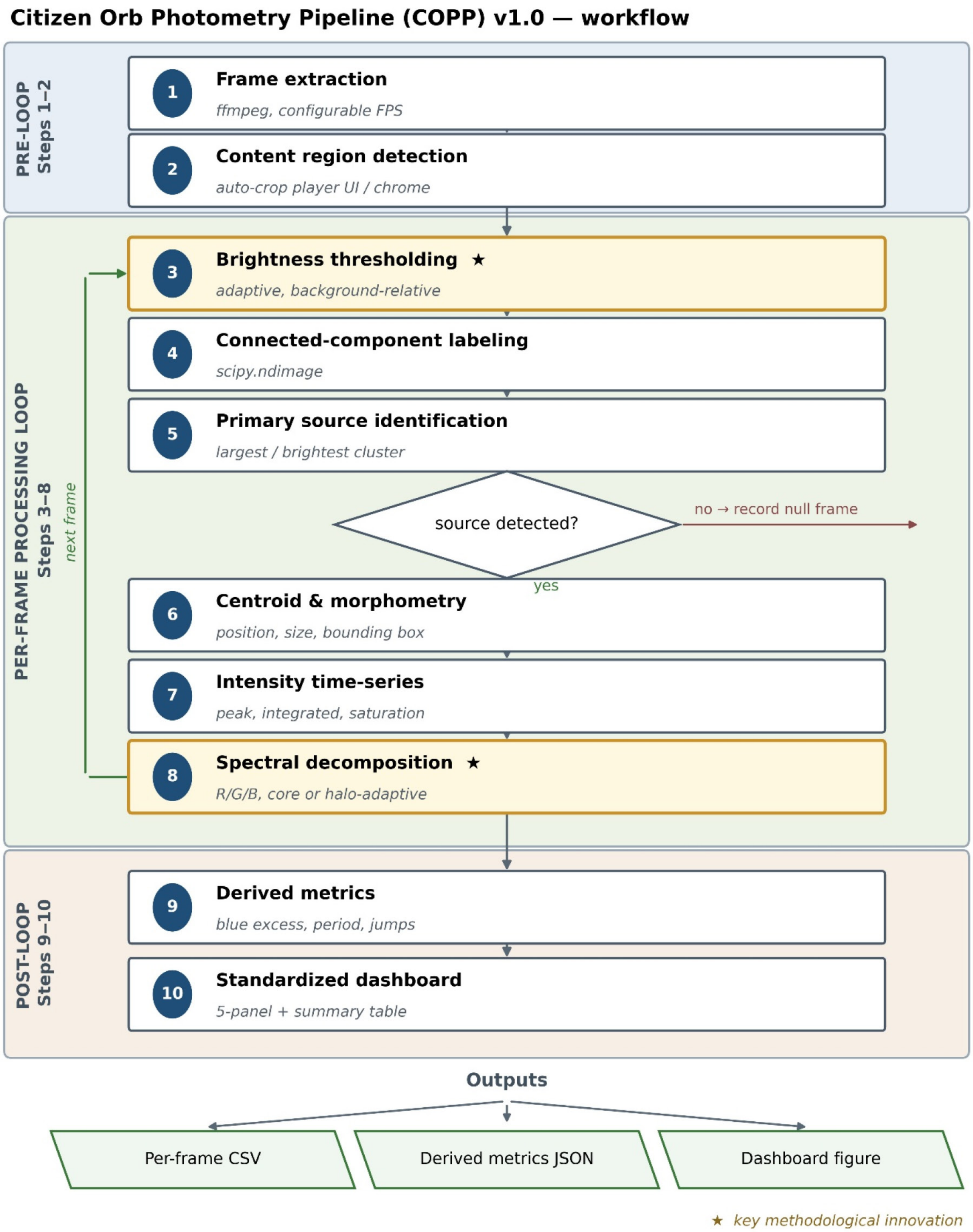

Figure 1. COPP v1.0 Pipeline Workflow in ISO 5807 Flowchart Notation, Showing the Pre-loop Phase (Steps 1–2), Per-frame Processing Loop (Steps 3–8) with Adaptive Source Detection Decision Point, and Post-loop Temporal Analysis and Output Generation (Steps 9–10). Legend identifies symbol types: rounded rectangles (start/end), rectangles (process), diamonds (decision), parallelograms (input/output), and starred items (key innovations).

Step 5: Primary Source Identification

The primary ALP source is identified as the largest connected component whose peak brightness exceeds 1.3 times the adaptive threshold. The size criterion selects the dominant luminous feature; the peak brightness criterion rejects diffuse background features that may exceed the threshold over large areas but lack the concentrated brightness characteristic of ALP sources.

Step 6: Morphometry

For the identified primary source, COPP computes brightness-weighted centroid coordinates (providing subpixel positional accuracy proportional to signal-to-noise ratio), total pixel count (apparent size), and bounding box dimensions (horizontal and vertical extent). The brightness-weighted centroid is more robust to asymmetric halo structures than a geometric centroid.

Step 7: Intensity Measurements

Three intensity metrics are computed per frame: peak intensity (maximum R+G+B sum of any single pixel in the source), integrated intensity (sum of R+G+B across all source pixels), and saturation fraction (proportion of source pixels where any single channel exceeds 250 DN). The saturation fraction is the gating parameter for the adaptive spectral measurement in Step 8.

Step 8: Adaptive Spectral Channel Decomposition

This is the central methodological innovation of COPP. Consumer cameras record in three broadband channels (Red, Green, Blue) spanning approximately 600–700 nm, 500–580 nm, and 420–500 nm, respectively. While these channels lack the spectral resolution of diffraction grating spectrometers, they provide coarse constraints on the dominant spectral character of luminous sources within a single capture session.

Calibration Limitations

It is essential to state clearly what consumer RGB photometry can and cannot establish. COPP operates on in-camera processed sRGB data, not linearized RAW sensor values. The camera imaging pipeline applies auto-exposure, auto-white-balance, gamma correction (typically sRGB gamma approximately 2.2), tone mapping, demosaicing, and lossy compression before producing the frames COPP analyzes. These transformations are nonlinear, device-specific, and generally irreversible without access to RAW data. Consequently, per-pixel DN values are not physically calibrated intensity measurements, and RGB channel ratios are not stable spectral proxies across different cameras, exposure settings, or white-balance states. COPP's spectral metrics (channel means, blue excess) should be interpreted as relative indicators within a single capture session, not as absolute physical measurements comparable across devices. The spectral classifications reported in this paper (cool/ionized vs warm/thermal) are indicative rather than definitive and should be validated against calibrated spectrometric measurements before physical conclusions are drawn. Future versions of the pipeline should incorporate RAW linearization where available, inverse gamma correction, camera spectral sensitivity (CSS) estimation, and normalized chromaticity coordinates (e.g., (B minus R) divided by (R+G+B), or CIE xy) to reduce exposure and device dependence.

The challenge is that bright ALP sources frequently saturate the sensor, driving all three channels to their maximum value (255 DN for 8-bit encoding) and destroying spectral information in the source core. COPP addresses this through adaptive measurement region selection. When the saturation fraction is below 0.3 (fewer than three in ten source pixels are saturated), spectral channels are measured as the mean R, G, and B values across all source pixels (core measurement). When the saturation fraction equals or exceeds 0.3, spectral channels are measured from the unsaturated halo region: pixels belonging to the source cluster that are in the brightness range 30–200 DN and are not individually saturated (halo measurement). This approach recovers spectral information that would otherwise be lost to saturation, and critically, enables cross-case comparison between saturated and unsaturated captures of the same phenomenon class. However, halo-derived spectra may be contaminated by optical point-spread function (PSF) wings, chromatic aberration, lens flare, and demosaicing artifacts. Characterizing these optical contributions on control targets (e.g., bright stars or point lights captured by the same device) is an important validation step for future work.

COPP reports two spectral metrics per frame. The blue excess in absolute DN (B minus R) provides a within-capture indicator of relative spectral shift. The normalized blue excess ((B minus R) divided by (R+G+B)) provides a ratio metric that is more robust to exposure variation and more comparable across captures, though still subject to the camera pipeline caveats noted above.

Step 9: Derived Temporal Metrics

From the per-frame time series, COPP computes several derived metrics. Position drift is the total range of centroid displacement in X and Y. Position jumps are frame-to-frame centroid displacements exceeding 30 pixels. Intensity variation is the ratio of maximum to minimum peak intensity. Pulsation analysis includes FFT-based power spectrum estimation and local maximum detection for quasi-period identification. Cross-correlations between size, intensity, blue excess, and position are computed to identify coupled physical behaviors. A Runs test (Wald–Wolfowitz) on the intensity time series quantifies whether bright and dim episodes cluster non-randomly. Burst episodes are identified as contiguous segments exceeding the mean plus 0.5 standard deviations of peak intensity.

Temporal and Kinematic Caveats

In the current implementation, time-domain analyses (FFT, autocorrelation, Runs test) operate on frame indices rather than true timestamps. For constant-framerate (CFR) video, frame indices are proportional to elapsed time, and periodicities can be converted to seconds by dividing by the known frame rate. For variable-framerate (VFR) video, frame indices introduce non-uniform temporal sampling, and analyses should properly use true timestamps with resampling to uniform time or methods designed for unevenly sampled data, such as Lomb-Scargle periodograms (Lomb, 1976; Scargle, 1982) or singular spectrum analysis. The current results report periodicities in frames; conversion to seconds requires confirmation of uniform temporal sampling, which we do not verify in this version. Additionally, position drift and position jumps reflect apparent motion in the image plane, which combines true source motion with camera motion (handheld shake, pan, jitter). The current pipeline does not perform camera motion compensation via background feature registration. Kinematic inferences (drift, jumps, non-ballistic motion) should therefore be interpreted cautiously, particularly for handheld captures, and validated by future implementations incorporating global motion stabilization. Auto-exposure and auto-white-balance adjustments by the camera firmware can also produce quasi-periodic intensity and color variations unrelated to the source; distinguishing these from genuine source pulsation requires either locked exposure settings or statistical separation of camera-induced and source-induced variation.

Step 10: Standardized Output

COPP produces three standardized outputs for each analyzed video, described in Table 1. The identical output format across all cases enables direct visual and quantitative comparison.

DEMONSTRATION: THREE-CASE COMPARATIVE ANALYSIS

We demonstrate COPP through application to three independent ALP video captures selected to span a range of observational conditions: source distance (near and far), sensor saturation state (saturated and unsaturated), geographic location (East Asia, Western Europe, Central Europe), and capture year (2011, 2021, 2025). This comparative analysis is intended as an illustrative demonstration of the method's behavior and outputs; it does not constitute formal validation in the statistical sense. True formal validation—including negative controls, synthetic positive controls, sensitivity analysis, and comparison against calibrated instruments—is identified as future work below.

Case 1: Taiwan Coast, March 28, 2021

A self-luminous orb was observed hovering over the ocean from a coastal location in Taiwan at night. The observer (the author) recorded the phenomenon on a mobile phone until the battery was exhausted. The video was preserved as a screen recording of the original capture. The orb appeared as a small, bright point source against a very dark background (median background brightness: 1 DN), allowing direct core spectral measurement without saturation (saturation fraction: 0.00).

COPP detected the orb in 178 of 246 extracted frames. Full per-frame results are shown in Figure 2. Key findings: apparent size ranged from 3 to 57 pixels with a mean of 23 pixels; peak intensity ranged from 66 to 764 DN (11.6-fold variation); blue excess was +3.7 ± 4.3 DN (cool, blue-shifted emission); position drift was 275 by 225 pixels with

Table 1. COPP Standardized Output Specification.

Output	Contents	Description
Per-frame data table (CSV)	Frame, time, centroid X/Y, size, extent X/Y, peak intensity, integrated intensity, saturation fraction, R/G/B channels, blue excess, spectral source	One row per frame. All Step 6-8 measurements. Machine-readable for statistical analysis.
Photometric dashboard (PNG)	Panel 1: Trajectory. Panel 2: Peak intensity. Panel 3: Spectral channels (R, G, B). Panel 4: Blue excess (B-R). Panel 5: Apparent size. Panel 6: Summary metrics.	Six-panel visualization of per-frame measurements. Identical layout for every case.
Signal structure dashboard (PNG)	Panel 1: Intensity with burst overlay. Panel 2: Autocorrelation function. Panel 3: FFT power spectrum. Panel 4: Size-intensity scatter. Panel 5: Inter-burst gap distribution. Panel 6: Statistical summary.	Six-panel visualization of Step 9 derived temporal metrics. Tests whether the intensity pattern is random or structured.

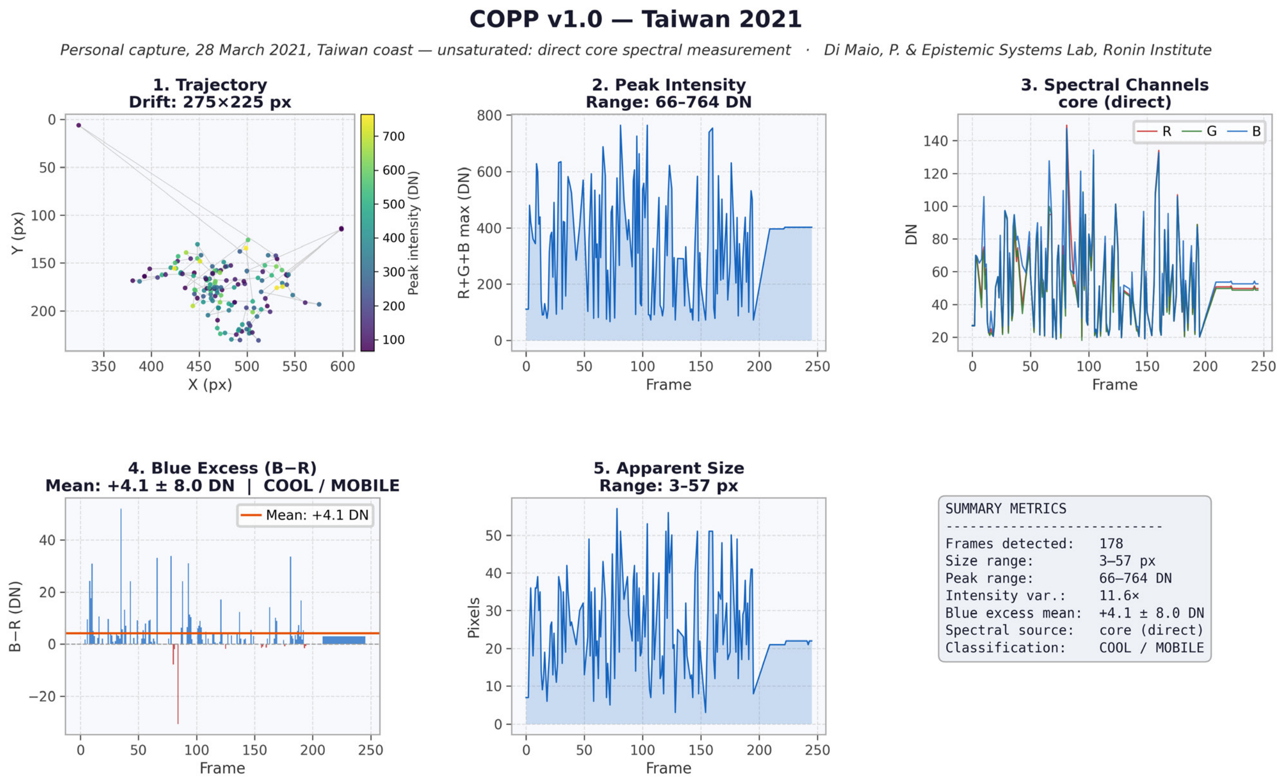

Figure 2. COPP Photometric Analysis: Taiwan Coast, March 28, 2021. Six panels showing: (1) centroid trajectory across the frame, colored by peak intensity—the orb drifted 275 × 225 pixels with 14 sudden position jumps; (2) peak intensity time series showing high variability (66–764 DN, 11.6× range) indicating genuine pulsation; (3) spectral channels R, G, B measured directly from the unsaturated source core; (4) blue excess (B minus R) with positive mean (+3.7 DN) indicating cool, blue-shifted emission; (5) apparent size varying 3–57 pixels, correlated with intensity; (6) summary metrics. Source: personal capture, unsaturated—spectral measurement from core (direct).

14 position jumps exceeding 30 pixels; and size-intensity correlation was r = 0.808. FFT analysis revealed dominant periods at 2.4, 7.1, and 8.5 frames.

Case 2: United Kingdom, 2011

A luminous orb was recorded at close range and posted to YouTube (identifier: XFhsCvBSMfw). The source was sufficiently bright to saturate the camera sensor across a large portion of the frame (saturation fraction: 0.32), requiring halo-based spectral measurement.

COPP detected the orb in all 71 frames. Full per-frame results are shown in Figure 3. Key findings: apparent size ranged from 143,485 to 328,369 pixels (sensor-saturating); peak intensity was constant at 765 DN (the sensor ceiling); blue excess measured from the halo was -75.3 plus or minus 3.4 DN (warm, amber-shifted emission); position drift was less than 5 pixels (stationary); the orb exhibited a sudden size expansion in the final frames, with saturated core area doubling between consecutive frames. Signal structure analysis was inconclusive due to the flat-topped intensity profile imposed by sensor saturation.

Case 3: Poland, 2025

A luminous orb was recorded at close range and posted to YouTube (identifier: Oe2olG9i3I8). Like the UK case, the source saturated the sensor (saturation fraction: 0.35), requiring halo-based spectral measurement.

COPP detected the orb in all 71 frames (66 frames of primary segment plus 5 frames of a distinct secondary segment). Full per-frame results are shown in Figure 4. Key findings for the primary segment: apparent size ranged from 67,154 to 74,303 pixels; blue excess was -77.1 plus or minus 3.7 DN (warm, amber-shifted); position drift was less than 5 pixels (stationary). A mid-video pulse was detected in which apparent size increased 4.8% simultaneously with blue excess shifting from -75 to -85 DN (warmer), demonstrating correlated size-color modulation.

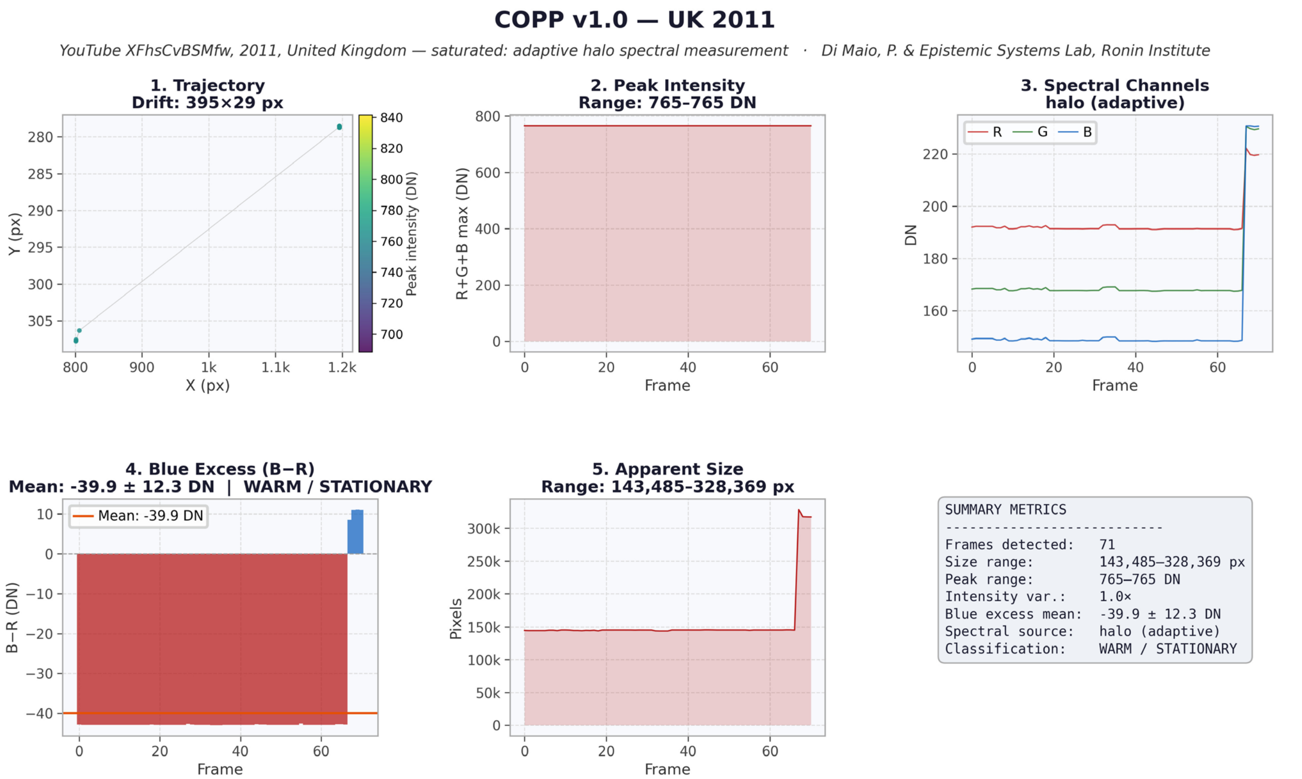

Figure 3. COPP Photometric Analysis: United Kingdom, 2011. Six panels showing: (1) centroid trajectory—the orb remained stationary throughout (drift less than 5 pixels, zero position jumps); (2) peak intensity flat at the sensor ceiling of 765 DN throughout, indicating sensor saturation; (3) spectral channels R, G, B measured from the unsaturated halo region surrounding the saturated core (adaptive halo measurement); (4) blue excess (B minus R) with negative mean indicating warm, amber-shifted emission from the halo; (5) apparent size showing a sudden expansion event in the final frames, with saturated core area doubling; (6) summary metrics. Source: YouTube XFhsCvBSMfw, sensor saturated—spectral measurement from halo (adaptive).

RESULTS

Table 2 summarizes the principal quantitative results across all three cases, organized by measurement category.

Spectral Consistency Across Cases

The most significant finding of the comparative analysis, presented side by side in Figure 6, is spectral consistency across all three cases despite dramatic differences in observational conditions. The Taiwan orb, measured directly from the unsaturated core, shows mean RGB values of (51.9, 51.1, 56.1) DN, giving a slight blue excess. The UK and Poland orbs, measured from the unsaturated halo surrounding the saturated core, show mean RGB values of approximately (183, 155, 107) and (182, 155, 107) DN, respectively. While the absolute brightness values and the channel ordering differ between the core-measured and halo-measured cases, all three sources exhibit measurable emission across the full visible range, with channel-dependent intensity patterns indicative of broadband emission rather than narrow-line emission from a single atomic species. The property shared across cases is broadband character rather than channel ordering; the difference in ordering is addressed below. Given the calibration limitations discussed in the Calibration Limitations section, this spectral overlap is suggestive of a common emission mechanism but cannot be considered definitive without calibrated spectrometric confirmation. The consistency is nonetheless notable given that the three captures were made by different cameras in different countries over a fourteen-year span.

The apparent difference in blue excess between the Taiwan case (+3.7 DN) and the UK/Poland cases (-75 to -77 DN) may be attributable to several factors: the different measurement regions (core vs. halo), atmospheric Rayleigh scattering over longer optical paths, different camera white-balance settings, or genuine physical differences in emission temperature. Disentangling these contributions requires either calibrated instruments or RAW camera data

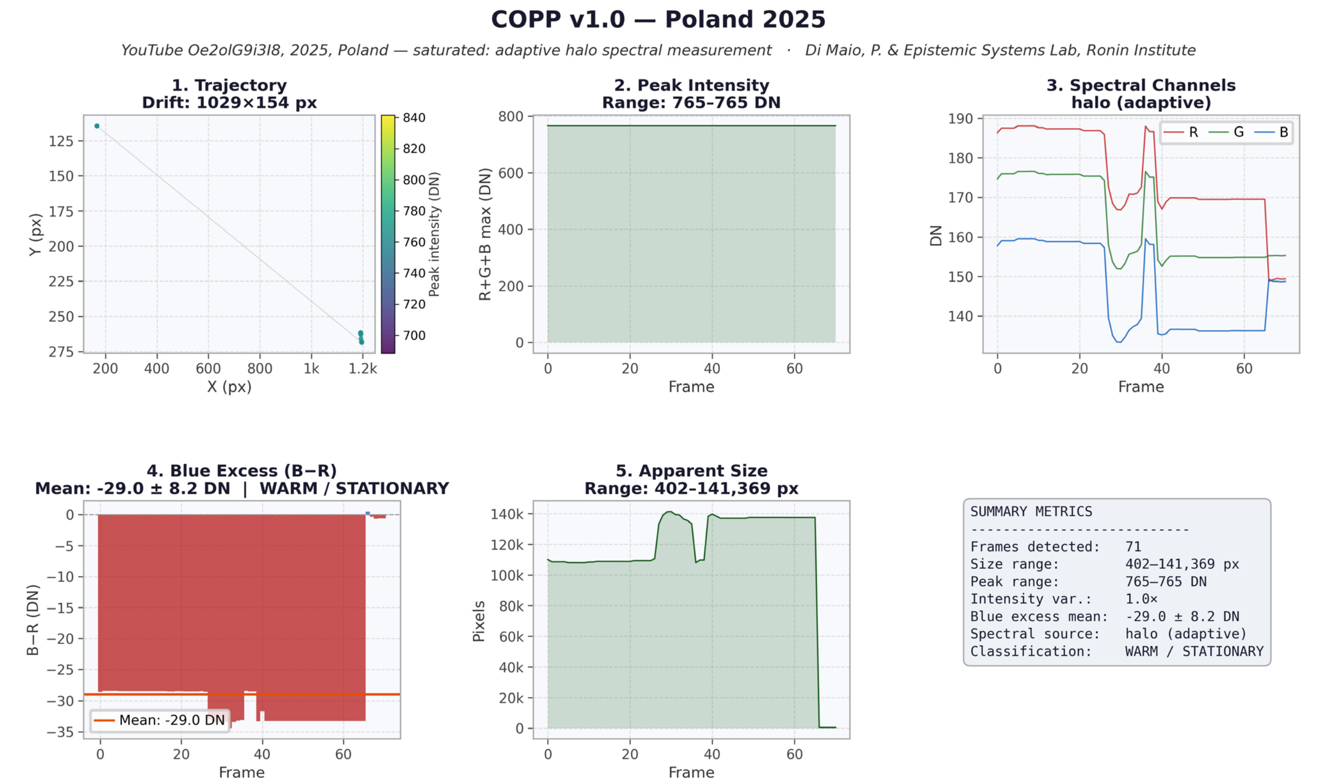

Figure 4. COPP Photometric Analysis: Poland, 2025. Six panels showing: (1) centroid trajectory—the orb remained stationary throughout (drift less than 5 pixels, zero position jumps); (2) peak intensity flat at the sensor ceiling of 765 DN, indicating sensor saturation throughout; (3) spectral channels R, G, B measured from the unsaturated halo region surrounding the saturated core (adaptive halo measurement); (4) blue excess (B minus R) with negative mean indicating warm, amber-shifted emission, with a mid-video pulse where the blue excess shifts to approximately −85 DN (warmer); (5) apparent size showing the correlated size pulse—apparent size increased 4.8% simultaneously with the color shift, demonstrating coupled size-color modulation; (6) summary metrics. Source: YouTube Oe2olG9i3I8, sensor saturated—spectral measurement from halo (adaptive).

with known spectral sensitivity functions. The normalized blue excess ((B minus R)/(R+G+B)) partially mitigates exposure dependence but does not resolve white-balance or camera-sensitivity confounds.

Signal Structure: Taiwan Case

The Taiwan case provides the richest signal structure data because the source did not saturate the sensor, preserving the full dynamic range of intensity variation (Figure 5). Three lines of evidence establish that the intensity pattern is non-random and physically structured:

First, the size-intensity correlation (r = 0.808) demonstrates that brightness increases are accompanied by physical expansion of the source, consistent with plasma emission from a volume whose size varies with energy input. Second, the size-blue excess correlation (r = 0.323) demonstrates that larger, brighter states exhibit a slight blue shift, consistent with higher excitation temperatures producing shorter-wavelength emission. Third, 30 discrete bright episodes were identified with a mean duration of 1.6 frames and a mean inter-episode gap of 4.1 plus or minus 2.6 frames, with FFT analysis revealing dominant periodicities at 2.4, 7.1, and 8.5 frames.

The temporal analysis operates on 178 detected frames, which is representative of typical citizen science capture length. Frequency resolution scales with sample size; the periodicities reported here should therefore be treated as indicative of quasi-periodic behavior rather than precise spectral peaks. Confirmation using longer recordings or aggregated multi-event datasets is a clear priority for future work (see Near-Term: Calibration and Robustness, below).

Signal Structure: UK and Poland Cases

The UK and Poland cases yielded inconclusive signal structure analysis. This null result is itself informative:

Table 2. Summary of Key Quantitative Results From COPP Analysis of Three ALP Captures.

Metric	Taiwan 2021	UK 2011	Poland 2025
Source	Personal capture	YouTube XFhsCvBSMfw	YouTube Oe2olG9i3I8
Distance class	Far (est. >500 m)	Close (est. <10 m)	Close (est. <10 m)
Frames analyzed / detected	246 / 178	71 / 71	71 / 71
Apparent size (pixels)	3–57	143,485–328,369	67,154–74,303
Sensor saturation	None (0.00)	Partial (0.32)	Partial (0.35)
Position drift (px)	275 x 225	< 5 x 5	< 5 x 5
Position jumps (>30 px)	14	0	0
Peak intensity range (DN)	66–764	765 (saturated)	765 (saturated)
Intensity variation	11.6x	1.0x (clipped)	1.1x (clipped)
Measurement source	Core (direct)	Halo (adaptive)	Halo (adaptive)
Blue excess B-R (DN)	+3.7 +/- 4.3	-75.3 +/- 3.4	-77.1 +/- 3.7
Spectral class (indicative)*	COOL / Ionized	WARM / Thermal	WARM / Thermal
Size x Intensity corr.	r = 0.808	N/A (saturated)	N/A (saturated)
Dominant periods (frames)	2.4, 7.1, 8.5	N/A	N/A
Motion class	MOBILE	STATIONARY	STATIONARY

Note. * Spectral classifications are indicative only, derived from uncalibrated RGB data. COOL/Ionized denotes positive blue excess suggestive of shorter-wavelength emission, consistent with ionized atmospheric gas; WARM/Thermal denotes negative blue excess suggestive of longer-wavelength emission, consistent with thermal radiation. These terms reflect relative spectral tendency, not confirmed physical state. Distance estimates for UK and Poland cases are approximate and based on visual inspection of the recordings.

sensor saturation imposes a flat ceiling on the intensity time series, destroying the dynamic range needed for temporal pattern analysis. The implication for citizen science methodology is clear: captures at moderate distance (which avoid sensor saturation) are more analytically valuable than close-range captures that appear subjectively more impressive. This counterintuitive finding should inform citizen observation protocols.

Behavioral Classification

COPP data support a preliminary two-axis descriptive classification of the three captures. This classification organizes cases by observable spectral and kinematic features as measured by the pipeline; it does not diagnose underlying physical mechanisms or distinguish between genuinely anomalous phenomena and conventional explanations, which requires calibrated multi-instrument observation and is identified as future work. On the spectral axis, the Taiwan case is tentatively classified as cool/ionized (positive blue excess, suggestive of atmospheric gas excitation) while the UK and Poland cases are tentatively classified as warm/thermal (negative blue excess in the halo, suggestive of lower-temperature emission). These classifications are indicative and subject to the calibration limitations discussed in the Calibration Limitations section. On the kinematic axis, the Taiwan case is mobile (275 by 225 pixel apparent drift with 14 apparent position jumps, noting that camera motion has not been separated from source motion) while the UK and Poland cases are stationary (drift less than 5 pixels, zero jumps). Whether these axes represent distinct subtypes of ALP, different observational presentations of a single phenomenon type, or artifacts of different camera and observation conditions remains an open question requiring calibrated multi-instrument observation.

DISCUSSION

Plasma Interpretation

The combined evidence from all three cases is consistent with, though not proof of, self-luminous atmospheric plasma. The indicators supporting this interpretation include: self-luminous emission (not reflected light, based on the absence of a correlated illumination source); broadband spectral emission across R, G, and B channels; correlated size-intensity variation in the Taiwan case (r = 0.808), where the source physically expands when it brightens, consistent with an emitting volume rather than a point source or reflection; blue excess in the distant case suggestive of ionized atmospheric gas emission; warm halo emission in the close cases suggestive of thermal emission;

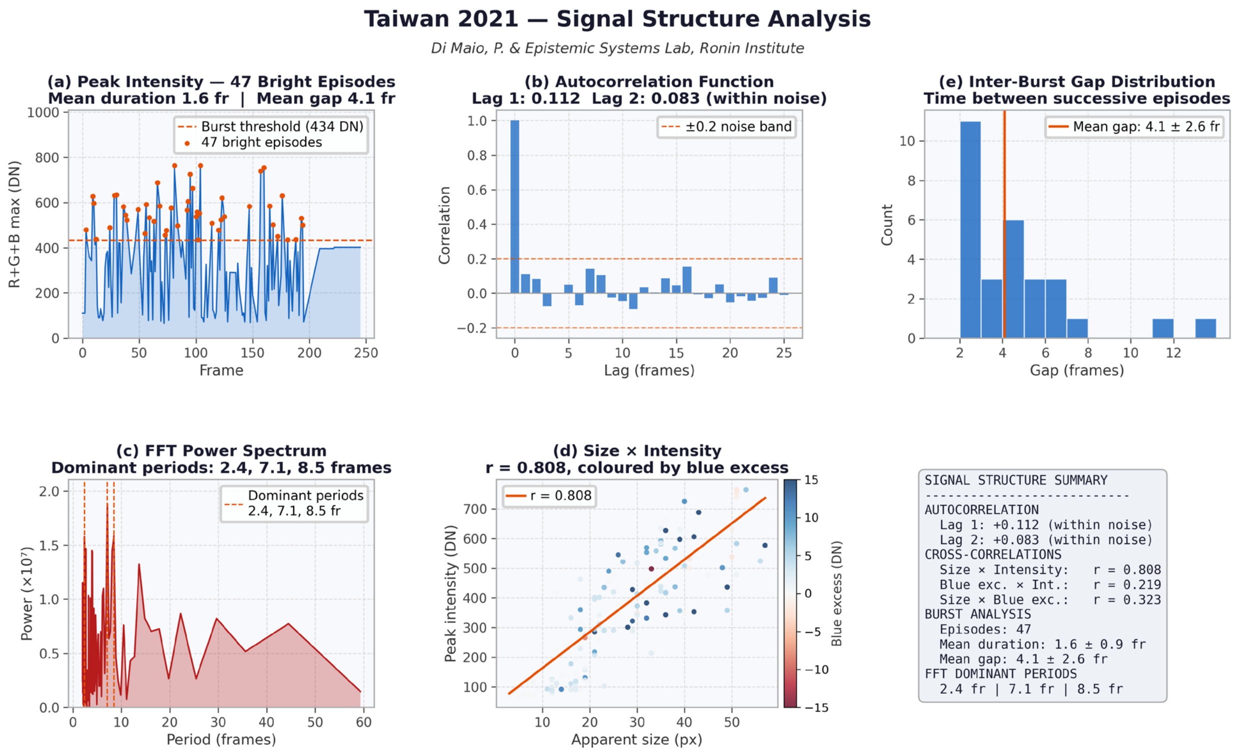

Figure 5. Signal Structure Analysis, Taiwan 2021. Six panels: (a) peak intensity time series with bright episodes marked—30 episodes identified above the burst threshold, with mean duration 1.6 frames and mean gap 4.1 frames; (b) autocorrelation function showing lag values within noise band, consistent with short-duration bursts rather than a single dominant periodic oscillation; (c) FFT power spectrum with dominant periodicities at 2.4, 7.1, and 8.5 frames, indicating quasi-periodic pulsation; (d) size-intensity scatter colored by blue excess, showing strong positive correlation (r = 0.808)—the source physically expands when it brightens, consistent with an emitting volume; (e) inter-burst gap distribution showing the time between successive bright episodes; (f) statistical summary including autocorrelation lags, cross-correlations, and burst statistics.

and persistent hovering behavior with, in the Taiwan case, apparent non-ballistic motion. These characteristics are broadly consistent with the physical parameters established for Hessdalen-type phenomena by Teodorani (2004) and with the electrically active atmospheric layer model proposed by Paiva (2021). However, definitive identification as plasma requires calibrated spectroscopy capable of resolving emission lines, which is beyond the capability of consumer RGB photometry.

Limitations

Several significant limitations constrain the conclusions that can be drawn from COPP analysis of consumer video. First, RGB values from in-camera processed video are not physically calibrated: autoexposure, auto-white-balance, gamma correction, tone mapping, and lossy compression all modify pixel values in device-specific, nonlinear, and generally irreversible ways. Spectral inferences from such data are indicative rather than definitive. Second, the halo-based spectral measurement, while conceptually sound, may be contaminated by optical PSF wings, chromatic aberration, lens flare, and demosaicing artifacts that produce color gradients unrelated to the physical emission spectrum. Characterization of these artifacts on control targets is needed. Third, kinematic measurements (position drift, jumps) combine true source motion with camera motion; without background-feature-based stabilization, these cannot be unambiguously attributed to the source. Fourth, time-domain analyses use frame indices as a proxy for time, which is valid for CFR video but introduces errors for VFR sources; periodicities should be confirmed using true timestamps and methods robust to uneven sampling, such as the Lomb-Scargle periodogram (Lomb, 1976; Scargle, 1982). Fifth, detection thresholds are heuristic and have not been subjected to sensitivity analysis, ablation testing, or statistical calibration (e.g., false-positive

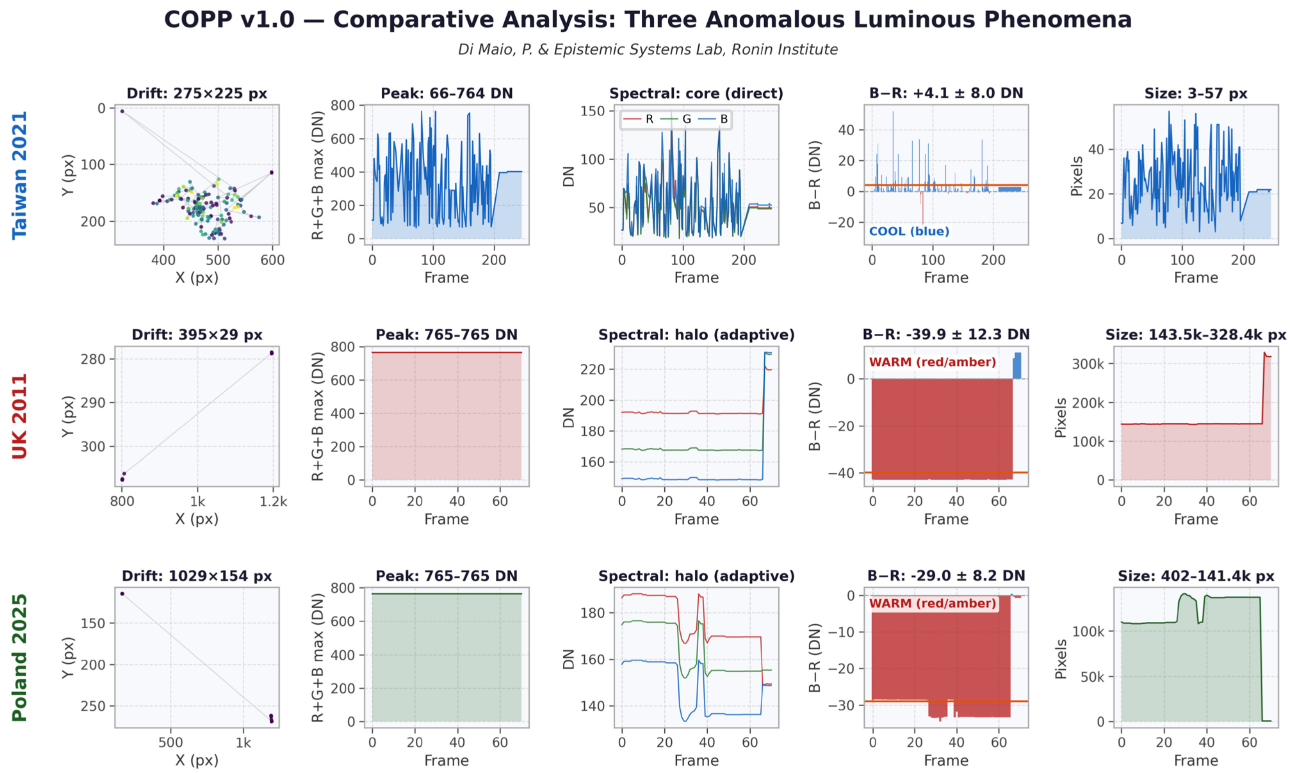

Figure 6. COPP Three-case Comparative Analysis. Each column shows one case (Taiwan 2021, UK 2011, Poland 2025) with identical five-row layout: (row 1) centroid trajectory colored by peak intensity; (row 2) peak intensity time series; (row 3) spectral channels R, G, B; (row 4) blue excess (B minus R) with mean indicated and spectral class labeled; (row 5) apparent size in pixels. Taiwan spectral measurement is from the unsaturated core (direct); UK and Poland spectral measurements are from the unsaturated halo (adaptive). Source videos: personal capture (Taiwan), YouTube XFhsCvB-SMfw (UK), YouTube Oe2olG9i3I8 (Poland).

rate estimation via negative controls). Sixth, the three-case illustrative set does not include negative controls (night sky without ALP, known stars, aircraft) or synthetic positive controls (injected signals with known parameters). Seventh, no comparison is made to established astronomical photometry toolkits such as astropy/photutils (The Astropy Collaboration et al., 2022) that incorporate well-characterized approaches to saturation, background subtraction, and color indices.

Spectral Overlap and Common Mechanism

The spectral channel overlap across all three cases, visible in Figure 6, row 3, is a notable finding that warrants cautious interpretation. Despite capture by different cameras, in different countries, over a fourteen-year span, and at distances ranging from tens of meters to possibly kilometers, the broadband RGB emission pattern shows consistent channel ordering. This consistency is suggestive of a common physical mechanism but must be weighed against the confound that all three captures were made at night with similar scene characteristics (bright source against dark sky), and consumer camera auto-white-balance algorithms may converge to similar settings under similar scene conditions. Confirmation of spectral commonality requires either calibrated spectrometric observation of multiple ALP events or, at minimum, COPP analysis of RAW video from cameras with known spectral sensitivity functions.

Implications for Citizen Science

COPP demonstrates that consumer video captures, traditionally dismissed as anecdotal evidence, contain quantitatively extractable photometric information. The pipeline's adaptive spectral measurement enables meaningful comparison between captures made under radically different conditions, a capability that has not previously been available to citizen observers. The counterintuitive finding that moderate-distance captures (which avoid sensor saturation) are more analytically valuable than close-range captures suggests that citizen observation protocols should be updated to recommend recording at a distance when possible, and to avoid zooming in to the point of sensor saturation.

FUTURE WORK

Intrinsic limitations of COPP v1.0 define a clear development roadmap organized into near-term improvements, medium-term extensions, and longer-term research directions.

Near-Term: Calibration and Robustness

The most critical improvement is reducing device dependence in spectral measurements. Where RAW sensor data are available, COPP should perform black-level subtraction, linearization (inverse gamma), demosaicing control, and white-balance normalization before computing spectral metrics. For processed sRGB sources (the majority of citizen captures), COPP should apply approximate inverse sRGB gamma, report normalized chromaticity coordinates ((B minus R)/(R+G+B) and CIE xy estimates) alongside raw DN values, and flag frames where auto-exposure or auto-white-balance metadata indicate mid-capture changes. Camera spectral sensitivity (CSS) estimation, even approximate, would enable camera-aware color normalization following approaches from the spectral reconstruction literature (e.g., Arad et al., 2020).

Detection thresholds should be replaced with statistically principled alternatives: percentile-of-background, robust z-scores, or extreme value theory (EVT) based cutoffs with controlled false-positive rates, following approaches demonstrated in low-SNR detection domains. A formal sensitivity analysis and ablation study across threshold parameters, bit depths, and scene types should accompany any threshold scheme.

Time-domain analyses must be converted to operate on true timestamps extracted from video container metadata, with resampling to uniform time for FFT and autocorrelation, or replacement by methods designed for unevenly sampled data such as Lomb-Scargle periodograms (Lomb, 1976; Scargle, 1982) or singular spectrum analysis (SSA). P-values for temporal tests should account for autocorrelation via block bootstrap or autoregressive modeling and be corrected for multiple testing when reporting several periodicities.

Near-Term: Motion Compensation and Controls

Camera motion compensation via background-feature-based stabilization (feature detection, homography estimation, affine warping) should be implemented as a preprocessing step before kinematic analysis, enabling separation of true source motion from camera jitter, pan, and dropped-frame artifacts. Only motion residuals after stabilization should be reported as source kinematics.

The demonstration set must be expanded to include negative controls (night sky footage without ALP, known astronomical sources such as bright planets and stars, aircraft with known trajectories) to estimate false detection and false classification rates. Positive synthetic controls should inject known signals (point sources with specified intensity profiles, pulsation patterns, spectral indices, and saturation levels) into real background frames to quantify COPP's recovery accuracy for each measured parameter.

The optical PSF and halo profile of each capture device should be characterized using control targets (bright stars, point lights at known distances) to distinguish physical emission halos from optical artifacts (PSF wings, chromatic aberration, lens flare, demosaicing color fringing). This characterization would validate or invalidate halo-derived spectral measurements on a per-device basis.

Medium-Term: Baselines and Community Tools

COPP should be benchmarked against established astronomical photometry toolkits, specifically astropy/photutils aperture and PSF photometry (The Astropy Collaboration et al., 2022), to quantify comparative accuracy in source detection, centroid precision versus SNR, intensity stability across frames, and color index consistency. Standard astronomical practices for handling saturation (aperture growth curves, PSF fitting with saturation masking) should be evaluated for applicability to ALP sources. A browser-based implementation of the pipeline is publicly accessible at https://copp-w.vercel.app/, enabling any citizen with a video recording and a browser to run the analysis.

Community capture guidelines should be formalized and distributed, incorporating the counter-intuitive finding that moderate-distance, unsaturated captures are more analytically valuable. Specific recommendations include lock exposure and white balance if the device permits; avoid digital zoom to prevent additional interpolation artifacts; include a reference light source in the field of view if possible for post-hoc calibration; and record in RAW or the highest-quality format available.

Development of a formal observation ontology using W3C standards would enable structured, machine-readable reporting of ALP observations, facilitating aggregation, search, and cross-referencing across citizen reports, institutional databases (NUFORC, MUFON, GEIPAN), and automated monitoring networks (Sky360, Project Hessdalen).

Longer-Term: Expanded Modalities and Cross-Validation

Extension to infrared modality using military-release FLIR footage would test COPP's framework on a different sensor type and spectral range. Integration of diffraction grating spectral data (from amateur spectrometers or calibrated field instruments) would enable chemical composition analysis through emission line identification. Correlation with geophysical parameters (seismic activity, electromagnetic field measurements, atmospheric electrical data, geological surveys) would test physical generation models such as piezoelectric discharge and electrically active inversion layers. An example of such integrated environmental analysis is provided by Houran et al. (2025), who conducted electromagnetic field measurements and environmental surveys at a reported anomalous phenomena site, demonstrating the feasibility of multi-parameter field characterization in this research domain. Cross-camera robustness testing using hyperspectral reference data rendered through multiple camera spectral sensitivity functions would quantify COPP's stability under realistic device variation. Machine learning classifiers trained on COPP-extracted features could enable automated ALP detection in continuous monitoring streams, and validation against calibrated Hessdalen AMS data (in collaboration with researchers who maintain these archives) would provide the strongest test of COPP's physical accuracy.

Next-Generation Capture Protocols and Multispectral Integration

Consumer imaging hardware is approaching a capability threshold relevant to COPP. Apple has disclosed exploration of multispectral imaging technology for future iPhone camera systems, targeting improved material detection and image processing fidelity (Hardwick, 2026). If multispectral capture becomes standard in consumer devices, COPP v2 could ingest per-pixel spectral data across more than three channels, substantially improving the physical interpretability of ALP emission signatures and reducing dependence on the RGB calibration caveats that constrain the current version.

A parallel development priority is standardized optical filter protocols for citizen scientists actively pursuing ALP field observation. Consumer clip-on optical filters—polarizing, neutral density, or narrowband—attached to smartphones could reduce image saturation for close-range captures and provide a calibration anchor for post-processing. A COPP filter mode, in which known filter transmission curves are applied as correction factors during spectral analysis, would enable more physically meaningful cross-case comparison. Establishing a recommended filter specification for the citizen ALP community is identified as a near-term collaborative development target.

These directions—multispectral ingestion and filter-calibrated capture—represent the primary hardware-side development pathway for COPP v2, complementing the software-side improvements described in the preceding Future Work subsections.

CONCLUSION

The Citizen Orb Photometry Pipeline establishes that consumer video recordings of anomalous luminous phenomena contain extractable photometric information amenable to standardized computational analysis. The three-case comparative analysis demonstrates broadband spectral consistency across observations made in different countries, years, and conditions, which is suggestive of a common physical mechanism though subject to the significant calibration caveats inherent in uncalibrated consumer RGB data. The Taiwan case provides evidence of non-random temporal structure, including correlated size-intensity expansion ($r = 0.808$), a correlation between size and blue excess ($r = 0.323$), and quasi-periodic pulsation. These temporal findings, which depend on intensity ratios rather than absolute calibration, are more robust to device confounds than spectral conclusions.

COPP v1.0 should be understood as a first-generation methods demonstration that establishes feasibility and identifies a clear development roadmap. Substantial improvements in calibration rigor (RAW processing, CSS normalization, inverse gamma), kinematic analysis (camera motion compensation), temporal analysis (true timestamp extraction, Lomb-Scargle), threshold calibration (statistical false-positive control), and validation (negative and synthetic controls, astronomical photometry baselines) are needed before COPP's spectral and kinematic claims can be considered definitive. Nevertheless, the pipeline addresses a documented tooling gap in citizen ALP observation, and its standardized outputs provide a foundation upon which these improvements can be built. The code, per-frame data, and source videos for all three cases are released with this paper to enable independent replication and alternative analyses. Readers are invited to use the online COPP tool, evaluate it, and test it. Contact the author for further development. The COPP v1.0 pipeline demo, available at https://copp-w.vercel.app/, is a working prototype; the results reported in this paper should be considered work in progress, based on ongoing analysis of three captures available to the author at the time of writing. More detailed metrics require thorough evaluation against larger and more varied datasets before they can be considered reliable or consistent at scale. We anticipate ongoing refinement of the measurement procedures of the pipeline and its demo implementation and to derive reliable statistics in future versions, in particular the temporal analysis, which will be reimplemented on true timestamps using methods appropriate to unevenly sampled data.

CONFLICTS OF INTEREST

The author has no conflicts of interest to disclose.

DATA AVAILABILITY

The dataset is now public here https://zenodo.org/records/22153927. The pipeline code and per-frame data for all three cases are released with this paper; the two third-party source videos are identified by their public URLs rather than redistributed.

AUTHOR NOTE

Citizen Orb Photometry Pipeline (COPP) v1.0: Standardized Photometric Analysis of Anomalous Luminous Phenomena in Consumer Video is also available on Protocols.io DOI: https://dx.doi.org/10.17504/protocols.io.n92ldo7eng5b/v1

REFERENCES

Arad, B., Timofte, R., Ben-Shahar, O., Lin, Y.-T., Finlayson, G., Givati, S., Li, J., Wu, C., Song, R., Li, Y., Liu, F., Lang, Z., Wei, W., Zhang, L., Nie, J., Zhao, Y., Po, L.-M., Yan, Q., Liu, W., ... Roomi, S. M. M. M. (2020). *NTIRE 2020 Challenge on Spectral Reconstruction from an RGB Image,* 1806–1822. Paper presented at 2020 IEEE/CVF Conference on Computer Vision and Pattern Recognition Workshops, Seattle, Washington, United States. https://doi.org/10.1109/CVPRW50498.2020.00231.

Barbi, M. (2025). Physical analysis of a reported missile – "orb" interaction in 2024: Momentum constraints, atmospheric drag, sensor artifacts, and theoretical caution. Preprint, arXiv:2512.04126v1.

Hardwick, T. (2026, January 7). Apple exploring multispectral imaging for future iPhones. *MacRumors*. https://www.macrumors.com/2026/01/07/apple-multispectral-imaging-future-iphones/

Hauge, B. G. (2010). Investigation & analysis of transient luminous phenomena in the low atmosphere of Hessdalen valley, Norway. *Acta Astronautica*, *67*(11–12), 1443–1450. https://doi.org/10.1016/j.actaastro.2010.01.019

Houran, J., Katz, D. L., Williamson, J., Koren, S. A., Wahbeh, H., & Woollacott, M. H. (2025). Magic flights or mind's eye? Further explorations of dimensional-slip narratives. *Journal of Anomalistics*, *25*(1), 61–118. https://doi.org/10.23793/ZFA.2025.061

Knuth, K. H., Ailleris, P., Agrama, H. A., Ansbro, E., Budinger, P. A., Cai, T., Canuti, T., Cifone, M. C., Cornet, W. B. Jr., Courtade, F., Dolan, R., Domine, L., Dini, L., Friscourt, B., Graves, R., Haines, R. F., Hoffman, R., Kayal, H., Little, S., ... Watters, W. A. (2025). The new science of unidentified aerospace-undersea phenomena (UAP). *Progress in Aerospace Sciences, 156*, 101097. https://doi.org/10.1016/j.paerosci.2025.101097

Lomb, N. R. (1976). Least-squares frequency analysis of unequally spaced data. *Astrophysics and Space Science*, *39*, 447–462. https://doi.org/10.1007/BF0064-8343

Morgan, P., & Tyson, D. (2024). Orb orientation and energy coupling in anomalous luminous phenomena [Field research report]. NRGscapes.

Paiva, G. S. (2021). Hessdalen lights produced by electrically active inversion layer. *Meteorology and Atmospheric-Physics*, *133*, 1447–1454. https://doi.org/10.1007/s00-703-021-00819-9

Scargle, J. D. (1982). Studies in astronomical time series analysis. II. Statistical aspects of spectral analysis of unevenly spaced data. *The Astrophysical Journal*, *263*, 835–853. https://doi.org/10.1086/160554

Strand, E. (1984). *Project Hessdalen 1984: Final technical report*. Østfold University College. https://old.hessdalen.org/reports/hpreport84.shtml

Teodorani, M. (2004). A long-term scientific survey of the Hessdalen phenomenon. *Journal of Scientific Exploration*, *18*(2), 217–251.

The Astropy Collaboration, Price-Whelan, A. M., Lim, P. L., Earl, N., Starkman, N., Bradley, L., Shupe, D. L., Patil, A. A., Corrales, L., Brasseur, C. E., Nöthe, M., Donath, A., Tollerud, E., Morris, B. M., Ginsburg, A., Vaher, E., Weaver, B. A., Tocknell, J., Jamieson, W., ... Zonca, A. (2022). The Astropy Project: Sustaining and growing a community-oriented open-source project and the latest major release (v5.0) of the core package. *The Astrophysical Journal, 935*(2), 167. https://doi.org/10.3847/1538-4357/ac7c74